Micro-Raman Spectroscopy for Detection of Label-Free and Oil Red O Labeled PEGylated Nanoliposomes in hCmec/D3 Cell Internalization Studies

Filip Gorachinov,[1,*] Petre Makreski,[2] Dushko Shalabalija,[1] Ljubica Mihailova,[1] Maja Simonoska Crcarevska,[1] Marija Glavas Dodov,[1] Katerina Goracinova,[1] Gligor Jovanovski,[3] Nikola Geskovski[1,#]

[1] Ss Cyril and Methodius University in Skopje, Faculty of Pharmacy, Institute of Pharmaceutcal technology, Majka Tereza 47, 1000 Skopje, Republic of North Macedonia

[2] Ss Cyril and Methodius University in Skopje, Faculty of Natural Sciences and Mathematics, Institute of Chemistry, Arhimedova 5, 1000 Skopje, Republic of North Macedonia

[3] Macedonian Academy of Science and Arts, Research Center for Environment and Materials, Bul. Krste Misirkov 2, 1000 Skopje, Republic of North Macedonia

* Corresponding author's e-mail address: filip.gorachinov@gmail.com

Corresponding author's e-mail address: ngeskovski@ff.ukim.edu.mk

RECEIVED: August 31, 2022 ✳ REVISED: February 4, 2023 ✳ ACCEPTED: February 6, 2023

THIS PAPER IS DEDICATED TO PROF. BRANKO KAITNER ON THE OCCASION OF HIS 80TH BIRTHDAY

Abstract: Rapid development of nanomedicines necessitates advancement in internalization techniques which can accurately distinguish between the complex environments of cells and nanocarriers. Internalization (or endocytosis) studies of oil red O labeled and label-free PEGylated-lecithin/cholesterol nanoliposomes was performed using micro-Raman spectroscopy. The C–O stretching vibrations and CCH scissoring bendings of naphthalene ring around 1225 cm^{-1} as well as the N=N stretching vibrations at 1377 cm^{-1} are prominent peaks absent from the label-free spectra which can be used for detection of internalized oil red O labeled nanoliposomes. Suitability of oil red O as a liposome marker was confirmed by stability studies of the incorporated dye and automated fluorescence cell counting. The C–C stretching region with a prominent wide band centered at 1080 cm^{-1} indicative of larger gauche conformer content typical for the lecithin-cholesterol nanoliposomes and the strong maximum at 980 cm^{-1} associated with O–C–C–N$^+$ stretching vibrations of the liposome polar head groups are important for studying label-free nanoliposome cell internalization.

Keywords: PEGylated nanoliposomes, oil red O labeled PEGylated-nanoliposomes, cell internalization studies, micro-Raman spectroscopy.

INTRODUCTION

NANOTECHNOLOGY is a rapidly developing field that demonstrates growing applications in many areas. Its subdiscipline, nano-engineered medicine, brings numerous clinical advantages and unique biological properties mainly due to the nanosize and specific physicochemical features of the evaluated biosystems. In this regard, vast technological advances in drug delivery and in biopharmaceutics emerge to act as therapeutic vehicles for molecules such as drugs, proteins, DNA and monoclonal antibodies.[1] Nanomedicines currently in use or under investigation include long circulating PEGylated liposomes, polymer nanoparticles or micelles, nanostructured lipid nanoparticles, lipid-polymer hybrid nanoparticles, and dendrimers. Due to their favorable physicochemical and biophysical properties, liposomes are considered as one of the most biocompatible nanocarriers capable of surpassing different biological barriers. In addition, multifunctional liposomal carriers equipped to support the EPR effect, also capable to transform into a "recognition" state and induce ligand-receptor interaction in different biological compartments, evolved to improve the lack of selectivity, increase the localization and cell internalization of conventional nanocarriers.[2–4]

Bioimaging technologies for cellular processing and intracellular fate of liposomes are crucial for optimization of these design approaches. However, understanding the nature of the interaction of nanoscale material with biological systems, their biodistribution and potential to

cross biological barriers, tissue accumulation and cell internalization, as accurate predictors of toxicity as well as effectiveness of therapeutics of interest, is restricted by the limitations of the available techniques. Most liable adopted methodologies for biological and biomedical imaging are fluorescence microscopy, flow cytometry, small-angle X-ray scattering and spectral bioimaging.[1]

Flow cytometry (fluorescence-activated cell sorting analysis) allows quantification of liposomal uptake but it cannot distinguish among the cell surface attached and internalized liposomes.[5] Localization studies may be performed using fluorescence microscopy in living or fixed cells stained with multiple fluorescent markers for endocytic compartments, organelles, or different endocytic pathways and incubated with fluorescently labelled liposomes. However, accurate localization is often hindered by low spatial and spectral resolution leading to overlapping of the fluorescent signals due to their proximity in the microscopic structure.[1,6,7] In order to achieve higher spatial resolution and segregate mixed fluorescence signals, confocal laser scanning microscopy (CLSM) is usually coupled with spectral imaging detector to secure high spectral resolution and resolve spatial contribution of each fluorophore. CLSM gives the 3D aspect of a sample with the exact spatial position of the nanoparticle and the spectral imaging measures the spectral information. Thus, a 3D emission spectral profile of each fluorophore spatially with a high spectral resolution is constructed, enabling the separation of fluorescent dyes in a multi-stained system.[8] Combined flow-cytometry and spectral bioimaging may also be applied to unravel the internalization mechanism and intracellular fate of liposomes and other nanomedicines.[9] However, fluorescent label induced changes in the physicochemical and biological properties as well as modifications of the cellular fate, dye leakage and/or reattachment to different structures, dye stability and photobleaching that lead to loss of tracking confidence or decrease of the signal over time are major limitations that cannot be easily resolved. Furthermore, the high energy wavelengths used to excite the fluorophores might damage the cells and cause the production of reactive oxygen species which is severe obstacle throughout time-course studies during which the toxicity imparted by reactive oxygen species (ROS) can become evident, impacting cell permeability and integrity.[7] The variety of problems introduced by fluorescent dyes need to be overcome by techniques that are able to compare and distinguish dye-free and dye-labeled nanocarriers. In order to circumvent the limitation of the fluorescent techniques, a viable approach delivered by use of other methods are explored.

Due to its high resolution and applicability to target live cells in both an aqueous environment and in fixed samples, confocal micro-Raman spectroscopy is commonly used for cell visualization. The technique enables noninvasive chemical imaging based on vibrational properties of functional groups within the sample and occasionally does not require compound labeling.[1,10] Direct visualization of components in the sample is usually performed by obtaining three-dimensional confocal Raman images and integrating the intensity of characteristic spectral bands measured at one location and at several sample layers.[11] Spectra can be obtained by focusing the laser beam at the point of interest or by mapping experiments that would be further processed by multivariate data analysis (chemometrics). Compared to the univariate methods, where information is extracted through the relative comparison of isolated band shifting and intensity changes observed in the spectra of individual samples, multivariate methods are more powerful and very accurate as they derive and compare the information from a number of whole spectra obtained from different sample points.[12]

In biological cells and other complex tissues, the observed spectra exhibit bands with various intensities and shapes that originate from the vibration of the various building blocks that constitute the biochemical components: nucleic acids, proteins, lipids, phospholipids, and carbohydrates. Due to the rich spectral content, apart from investigation of the molecular compositions and structures, the technique could be exploited to track the optical signals arising from internalized liposomes, provided that the uptake is sufficiently large. Considering the scarcity of data regarding the use of spontaneous confocal micro-Raman spectroscopy to study cell internalization of labeled and label-free nanomedicines,[13] the aim of this study was to test and highlight the potential of the technique for evaluation of the internalization of PEGylated-lecithin/cholesterol oil red O labeled and label-free liposomes in brain microvascular endothelial hCmec/D3 cell line. The approach represents an established *in-vitro* blood-brain barrier (BBB) model in the development of brain targeted drugs and drug delivery systems.

EXPERIMENTAL

Materials

Soybean lecithin (SL) was purchased from Vitalia, N. Macedonia. LIPOID PE 18:0/18:0-PEG 2000 (PEG) was donated from Lipoid, Germany. Cholesterol (CH) was purchased from Sigma Aldrich, Germany. Oil red O was purchased from Sigma-Aldrich, St. Louis, MO, USA. Methanol, chloroform, and formic acid were of HPLC grade purity and supplied from Merck, Germany. EndoGRO-MV Complete Culture Media Kit SCME004 (cell culture media) was purchased from Merck, Germany. Phosphate buffer (PB) with pH 7.4 was prepared ex tempore (Ph. Eur. 9).

Preparation of PEGylated Nanoliposomes and Oil Red O Labeled Nanoliposomes

Liposome dispersion was prepared according to the procedure outlined by Shalabalija et al.[14] SL (261.02 mg), CH (30 mg), PEG (50 mg) were dissolved in a 1 : 4 methanol : chloroform mixture (V/V). The organic solvents were removed under vacuum using a rotavapor (25 °C, 50 rpm, 50 mbar; Buchi 215 Switzerland). The obtained film was hydrated using PB pH 7.4 in four, consecutive three-step cycles (step 1: ultrasonification ULTRASONS-H, J.P Selecta; step 2: vortexing Tehtnika, EV-102; step 3: manual mixing at room temperature) and further submitted to high shear homogenization (Ultra-Turrax T25, IkaWerke, Germany). Then, the samples were left for 24h at 4–8 °C, and again homogenized at 6000 rpm for 3 minutes. Finally, the preparations were washed and concentrated in four consecutive cycles (Rotofix 32 - Hettich Zentrifugen, Germany) at 4500 rpm, 25 °C for 15 minutes using Vivaspin 20 ultrafiltration cuvettes 1000 kDa (Sartorius, Germany). The labeled liposomes were prepared with the previously stated procedure that was modified as described by Mozfari et al.[15] In brief, the Oil red (0.1 ml 25mM solution in chloroform) was added during the dissolution of the SL, CH, PEG in the 1 : 4 methanol:chloroform mixture (V / V) with no further changes in the liposome preparation procedure. The eluate from the last washing step was analyzed by UV spectroscopy in the 200–400 nm region (Carry 60, Agilent, USA) to confirm the absence of bands from free Oil red O. The stability of the encapsulated dye was analyzed after 7-days storage at 8 °C by washing and ultrafiltration of the labeled nanoliposomes and further UV scanning of the obtained eluate.

Determination of Particle Size, Size Distribution and Zeta Potential

Particle size and zeta potential (Zetasizer Nano Series, Nano-ZS, Malvern Instruments Ltd., UK) were measured in disposable transparent cuvettes at 25 °C following dilution of NL dispersion 1 : 5 (V / V) in 10 mM PB pH 7.4.

Cell Culture

Cell culture hCmec/D3 (human brain endothelial vasculature cells) was used as a model for blood-brain barrier translocation of the prepared nanoliposomes. The cells were maintained in EndoGRO-MV Complete Culture Media (MerckMilipore, Germany) on 37 °C, 10 % CO$_2$ and saturated humidity. The seeding was performed on a rat collagen coated sterile cell culture flasks and multiwall plates.

Internalization Studies

The cell internalization experiments were guided according to a method described by Mourtas et al. with slight modification.[16] In brief, cells were seeded in a rat collagen coated 6-well plate at a density of 1 × 10^6 cells/well and left overnight. The label-free and oil-red labeled liposomes were added to cell culture medium in concentration of 200 nM (calculated on liposomal lipids) for a period of 4 h. Untreated cells were liposome free samples and used as blanks. Afterward, the cells were triply washed with Dulbecco PBS (Thermo Scientific, USA) and detached from the wells using Trypsin-EDTA solution, and further washed with cell culture medium to remove the detachment reagent. The cells were again washed with Dulbecco PBS and were fixed using 10 % paraformaldehyde solution in PBS for 30 min. The fixed cells were washed three times with PBS and further stored on 4 °C until analyzed.

Fluorescent Microscopy

Luna fluorescence cell counter (Logos Biosystems, Republic of Korea) was used for quantification of the cell population internalized with Oil red labelled nanoliposomes. Twelve microliters of the fixed cell suspension in PBS, was transferred on cell counting slide and inserted in the instrument. The counting was performed in fluorescent cell counting mode using the following parameters: red channel excitation 20, red channel threshold 5, cell size gating 3–60 μm. The number of cells counted per run was 400–600 and the percent of cells with internalized nanoliposomes above the set threshold was calculated as an average of three counts.

Micro-Raman Spectroscopy

The micro-Raman spectra of the samples were collected on the LabRam 300 spectrometer (Horiba Jobin Yvon, USA) coupled to Olympus LMPlanFL confocal microscope by using the second harmonic of Nd:YAG laser (532 nm). The backscattered radiation (180° configuration) was analyzed with an 1800 lines / mm diffraction grating. Raman intensities were collected on a cooled CCD array detector. A long-distance × 50 objective (N.A = 0.5) with a working distance of 10.6 mm was selected. The pinhole of 500 μm and the slit of 100 μm were selected. No attenuation filter was used and the laser power on samples (0.99 mW) was measured by LaserCheck TM Handheld Power Meter (Coherent Scientific, Australia). The acquisition time was 12 seconds, and the accumulation number (number of scans) was set to 10 for each spectral collection. The fixed cell samples were drop-added on a microscope slide, which was further air-dried to a dry film while the nanoliposomes (labeled and label-free) were scanned as freeze-dried samples.

RESULTS AND DISCUSSION

Two different detection strategies, including label-free and label-mediated, were developed to achieve accurate analysis of liposome internalization in brain microvascular endothelial hCmec/D3 cell line and to evaluate the capacity

DOI.ORG/10.5562/cca3912

Croat. Chem. Acta 2022, *95*(4), 131–140

Table 1. *Z*-average hydrodynamic diameter (*n* = 3), polydispersity index (*PDI*) and zeta potential of the analyzed nanoliposomes.

Sample	*Z*-average *hD* / nm ± SD	*PDI* ± SD	ζ potential / mV ± SD
Nanoliposomes	106.20 ± 1.05	0.31 ± 0.03	−18.03 ± 1.52
Oil red labeled nanoliposomes	106.23 ± 1.85	0.29 ±0.02	−20.38 ± 1.36

of micro-Raman spectroscopy for direct detection of internalized liposomes without labels as well as detection of internalized oil red O labeled liposomes. Direct detection of internalized nanocarriers is increasingly attracting attention as it has the potential to simplify and accelerate testing of the toxicity and efficacy of nanocarriers. Introducing labels, which may enable specific detection without influencing physicochemical and biological properties of the nanocarriers, is also of specific interest for more accurate and rapid imaging of nanocarriers' biological fate.

Two types of nanoliposomes, non-labeled PEGylated lecithin/cholesterol and oil red O labeled PEGylated-lecitin/cholesterol liposomes, were prepared and the results from the *Z*-average hydrodynamic diameter (*hD*) (*n* = 3), polydispersity index (*PDI*) and zeta potential of nanoliposomes are presented in Table 1.

The results of zeta potential measurements, *Z*-average *hD* and *PDI* pointed to great resemblance between the prepared samples of labeled and non-labeled nanoliposomes. Similar parameters were measured one hour after incubation in biorelevant media used for cell culture internalization studies revealing minor differences, which confirmed their stability during the cell culture experiments.

To evaluate the internalization behavior of the nanoliposomes in the hCmec/D3 cells, an established fluorescent microscopy technique was employed using automated fluorescence cell counter capable of detecting Oil red O epifluorescence. After 4 h of exposure, Oil red O labelled nanoliposomes could be detected in 95.3 ± 4.2 % of the counted cells (*n* = 3). The Oil red O epifluorescence was clearly distinguishable from the background (Figure 1, a and b). The cells were intact, and neither cell necrosis nor toxicity were evidenced considering the short incubation time. In addition, the presence of cell aggregates in the samples was minimal, indicating towards negligible errors in the automated cell counting (Figure 1c).

The samples of labeled and non-labeled PEGylated-cholesterol/lecithin nanoliposomes, control hCmec/D3 cells and hCmec/D3 incubated with each of the samples (as described in the internalization experiments) (Figure 2 a–e) were measured and evaluated by micro-Raman spectroscopy.

The most prominent features in the Raman spectra of the hCmec/D3 cells (C) can be found in the C–H stretching region (3100–2800 cm^{-1}) and the fingerprint region
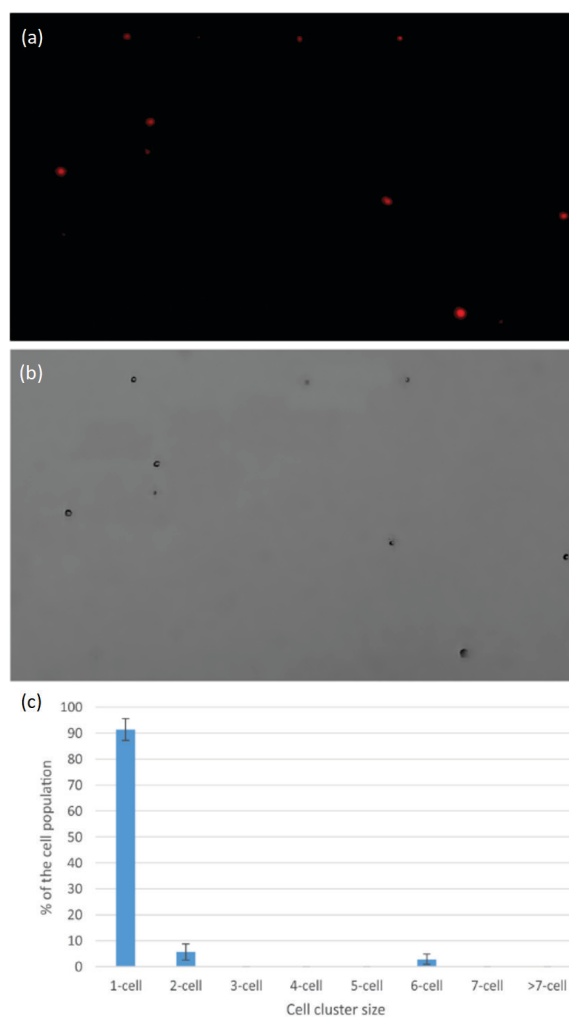

Figure 1. Microscopy image of hCmec/D3 cells after the internalization experiments with Oil red O labeled liposomes: (a) epifluorescence exposure; (b) phase contrast; (c) cluster size distribution of counted cell population.

(1700−900 cm^{-1}) (Figure 3, C). Details about the tentative band assignments are in agreement with the literature and are accordingly reported (Table 2). The Raman spectra of label-free liposomes (L), control cells (C) and cells incubated with internalized (label-free) liposomes (CL) are similar, but still exhibit notable spectral differences (Figure 3). The assignment of the bands extracted from these spectra are reported in Table 2 (first three columns). The Raman spectra of the liposome containing samples (L and CL) present characteristic bands assigned to the vibrations of the lipid tails (methylene C–C skeletal stretching modes of the trans and gauche conformations in the acyl chains of the lipids)[17] detected in the 1150–1030 cm^{-1} region with the strongest maximum at 1087 cm^{-1} and 1095 cm^{-1} in the L and CL spectrum, respectively. In addition, weak bands around
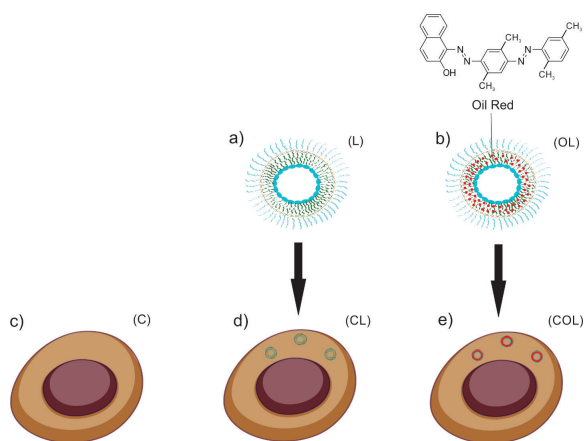
Figure 2. Schematic presentation of the experimental setup: (a) non-labeled PEGylated-cholesterol/lecithin nanoliposomes (L); (b) Oil Red O labeled PEGylated-cholesterol/lecithin nanoliposomes (OL); (c) control hCmec/D3 cells (C); (d) hCmec/D3 cells incubated with non-labeled PEGylated-cholesterol/lecithin nanoliposomes (CL); (e) hCmec/D3 cells incubated with Oil Red O labeled PEGylated-cholesterol/lecithin nanoliposomes (COL). The samples were further subjected to micro-Raman spectroscopy measurements.

1440 (L and CL) and 1300 cm^{-1} (L) from the CH$_2$ deformation modes[18,19] (twist and bending mode, respectively) were registered. Despite their weak intensity, these spectral features are very informative because no overlap with the bands of other structural units occurred. The symmetric C=C bond stretching[18] of cholesterol is manifested as a well-defined peak at 1657 (L) and 1656 cm^{-1}(CL). Three very prominent bands between 3100 and 2800 cm^{-1} are very important. Namely, the band at 2854 cm^{-1} (L and CL) and the bands at 2895 (L) and 2878 cm^{-1} (CL) are assigned to asymmetric and symmetric C–H methylene stretching, respectively.[19] Symmetric C–H stretching band of terminal methyl groups evolved at 2925 (L) and 2932 cm^{-1} (CL). The peak at 3015 cm^{-1} is attributed to the choline methyl asymmetric stretching mode and to Ar(C–H) stretching vibrations.[18,20] Both, the methylene C–C stretching and the methylene C–H stretching regions are good indicators of the liposome membrane order.[19,21,22] Spectral regions of 3000–2750 cm^{-1}; 1180–1000 cm^{-1}; 1300–1200 cm^{-1}; and 1500–1400 cm^{-1}, might also carry information about the PEG moieties (symmetric and antisymmetric stretching of PEG's methylene group);[22] C–O–C vibrations of polyethylene glycol chains trans and gauche conformation,[23,24] CH$_2$ twisting vibrations;[18,22] and CH$_2$–CH$_2$ symmetric and antisymmetric bending vibrations,[25] respectively. Many of these bands in the spectra of liposome containing samples (L and CL) overlap with phospholipid vibrations and cannot be clearly distinguished.

Oil red O is a lysochrome diazo dye that stains neutral triglycerides, fatty acids, cholesterol esters and some lipoproteins, and is used to monitor and understand physiological and pathophysiological events in lipid metabolism as well as excessive accumulation of lipids in tissues and cells as a key feature of several metabolic diseases.[26,27] Despite their high lipophilicity and preference for neutral lipids such as triglycerides and cholesterol esters, due to its amphiphilic properties and presence of polar groups, –OH and –N=N–, oil red O may also interact with the polar head groups of phospholipid and cholesterol molecules from the liposome bilayer, and therefore can be utilized to improve their visualization. Oil red O is often preferred over Sudan red IV dye due to more intense staining offering improved visualization capabilities, while maintaining similar physico-chemical properties and staining capacity.[28]

Only sparse data exists regarding the labeling of liposomes with Sudan red dyes.[29] Li *et al.* in 2007 pointed to the existence of hydrophobic interaction among Sudan IV and acyl chains of phosphatidylcholine, as well as to formation of hydrogen bonds with the lecithin head groups. More structurally complicated molecules from the Sudan red family dyes, with larger number of polar and lipophilic groups, like Oil red O, would potentially form more stable non-covalent bond complexes, which cannot be easily reversed. Further, larger molecules with greater steric effect will contribute to a lesser number of molecules internalized in the phospholipid bilayer. In that respect, it was calculated by the Langmuir isothermal equation that 314 lecithin molecules bind to one Sudan IV molecule, compared to 31 lecithin molecules bound to one Sudan II molecule in the Sudan red liposome complex, due to a lesser steric effect of Sudan II dye.[29] Compared to Sudan red IV, Oil red O molecule contains one additional methyl group in the para position in benzene, and is used as a lecithin/cholesterol liposome label that would result in a formation of a very stable non-covalent complex.

Our results confirmed the stability of the created oil red O PEGylated-lecithin/cholesterol liposome complex as there was no free dye present in the eluate after 7 days of storage (Figure S1). This was expected, as once entrapped in the lipid phase the partitioning out of Oil red O is unfavorable due to the dye's very low aqueous solubility. As expected, the most prominent bands (Table 2; Figure 4 in the Raman spectra of Oil red O emerged at 1228 cm^{-1} (naphtyl group C–O vibration and CCH scissoring bending of naphthalene ring),[30] 1377 cm^{-1} (N=N stretching vibration),[30,31] 1479 cm^{-1} (CH$_3$ bending asymmetric and symmetric),[32] and 1581 cm^{-1} (C–C stretching vibrations from the aromatic rings and N=N stretching vibration).[30] The Oil red O labeled liposome spectra resemble the Raman spectra of free analogues and all spectral bands of the Oil red O also appear in the Raman spectra of dye labeled liposomes

Table 2. Tentative assignment of the bands observed in the Raman spectra of: non-labeled PEGylated-cholesterol/lecithin nanoliposomes (L), hCmec/D3 control cells (C), hCmec/D3 cells incubated with non-labeled PEGylated-cholesterol/lecithin nanoliposomes (CL), Oil Red O (O), Oil Red O labeled PEGylated-cholesterol/lecithin nanoliposomes (OL), hCmec/D3 incubated with Oil Red O labeled PEGylated-cholesterol/lecithin nanoliposomes (COL).

L	C	CL	O	OL	COL	Assignment
3015 m						NCH$_3$ choline asymmetric stretch[18] and Ar(C–H) stretchings[20]
2925 vs	2937 vs	2932 s			2938 m	CH$_3$ asymmetric stretch and CH$_2$ asymmetric stretch[19,35]
2895 s	2878 s	2878 s				CH$_2$ symmetric stretch and CH stretch of lipids and proteins[19]
2854 s	2854 sh	2854 sh				
1657 m	1655 m	1656 w				C=C symmetric stretch, cholesterol[18]
			1607 m	1609 w	1609 w	ν(C–N) stretching in C=C–N=N[32]
			1581 m	1580 m	1580 w	C–C stretching vibrations from the aromatic rings and N=N stretching vibration[30]
1499 m		1481sh				CH$_2$ deformation mode, cholesterol[18]
			1479 m	1481 m	1480 m	CH$_3$ bending asymmetric and symmetric[31]
	1459 m	1455 m			1461 m	Uracil, cytosine ring stretching, CH deformations[44]
			1458 m	1453 sh	1447/1446 m	C–H in plane bending of extra benzene ring[38]
1440 vw		1446 vw				CH$_2$ bend (lecithin + cholesterol)[19]
			1377 s	1377 s	1377 s	N=N stretching vibration and C–H in plane bending, CH$_3$–Phenyl[31]
1369 w		1375 w				Amide III random coils[39]
1338 w		1339 w				CH$_2$/CH$_3$ wagging & twisting mode in collagen, nucleic acid & tryptophan[40]
			1338 m	1338 w	1338 m	CH bending[38]
1298 w						CH$_2$ twist[19]
	1266 vw			1253 vw		CH bending[38]
	1233 w					Amide III β-sheet[39]
		1227 w				Amide III random coils[39]
			1228 vs	1225 vs	1227 s	C–O stretching vibration and CCH scissoring bending of naphtalene ring[30]
			1203 m	1203 sh	1203 sh	CH bend oil red, δ(CH)[38,41]
			1188 m	1187 sh	1189 sh	CH bend oil red, δ(CH) + ν(C–N$_{azo}$)[41,42]
					1151 w	ν(C–N$_{azo}$), δ(CH)[41,42]
	1124 w					C–C stretching mode of lipids , trans conformers[19]
	1099 w					C–C stretch lipids, Isolated gauche conformers[19,43]
1087 s		1095 s				C–C stretch lipids region (lecithin), Isolated gauche conformers[17]
			1094 m	1095 m	1095 m	Aromatic CH bending in plane, δ(CH)[32]
	1066 w					Out of phase trans conformers, In phase trans conformers[17]
	1001 m	1001 w				Phenylalanine, C–C aromatic ring stretching[17]
			983 w	983 w	985 w	=N–Phenyl stretching[41]
981 m		981 m				O–C–C–N$^+$ stretching choline[17]
	935 m					C–C stretching mode of proline & valine & protein backbone (α-helix)/glycogen (protein assignment)[17]
	573 vw					Skeletal ring modes, Tryptophan/cytosine, guanine[43]
	481 w					out of plane ring deformations, guanine[44]

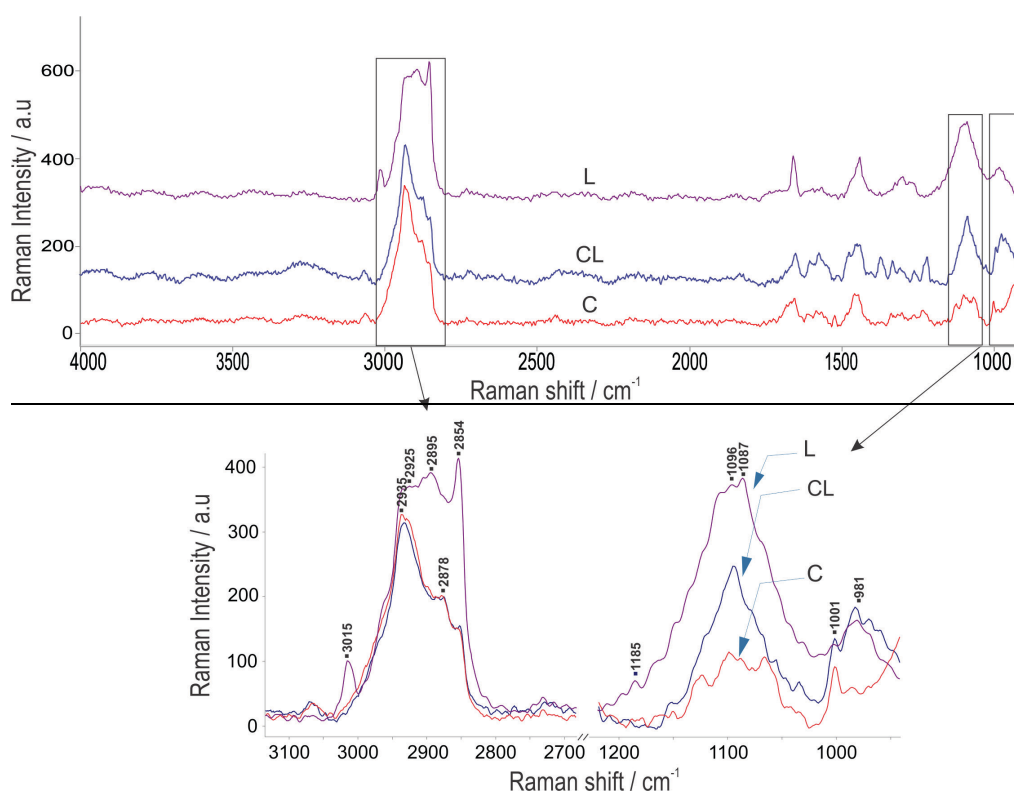Intensity codes: s − strong, m − medium, w − weak, sh − shoulder, v − very.

Figure 3. Raman spectra of: label-free liposomes (L); cells incubated with label-free liposomes (CL); and control cells (C) (top panel). The spectral regions of interest are marked in rectangles and further zoomed in and overlaid for better visualization (bottom panel).
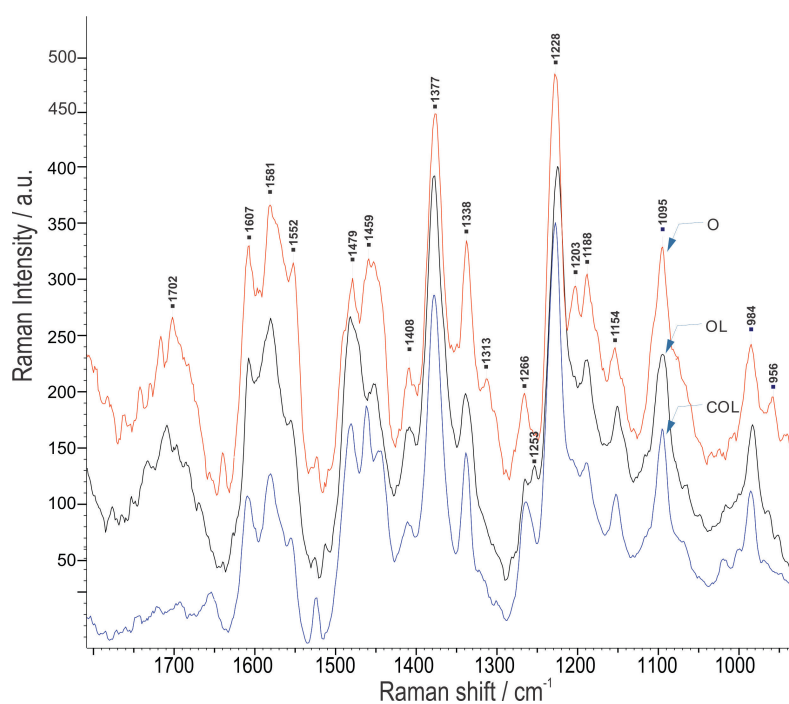

Figure 4. Raman spectra of Oil Red O (O); Oil Red O labeled liposomes (OL); and cells incubated with Oil Red O labeled liposomes (COL).

(Table 2; Figure 4). Changes in relative intensities of characteristic peaks (red shift of C–O stretching vibration from 1228 to 1225 cm^{-1}, abrupt decrease in the intensity of CH$_3$ deformation band at 1203 cm^{-1} and appearance of a new very weak peak at 1253 cm^{-1} (CH bendings), observed in the labeled liposo me (OL) spectra might be due to the interaction and orientation of oil red O molecules within the phospholipid bilayer.[29] In the Raman spectra of the cells incubated with oil red O labeled liposomes (COL) the internalization of the nanoparticles can be detected by several distinct peaks, of which two are the prominent and are not present in the label-free spectra (Table 2; Figure. 4; Figure 5), namely C–O stretching vibration and CCH scissoring bending of naphthalene ring[30] at 1227 cm^{-1} and N=N stretching vibration at 1377 cm^{-1}.

Although the resulting Raman spectra of the cells with internalized liposomes comprise superposition of bands from various cellular components and internalized structures within the focal volume, based on the differences among the spectra arising from non-labeled liposomes, free cells and the cells with internalized liposomes, several assumptions relevant to the internalization procedure are emphasized. Literature data point to potential differences in the spectra of the cells when performing spontaneous Raman spectra of different cellular regions due to heterogenous chemical distribution within a cell at different locations. One spot spectrum and univariate analysis cannot find an effective solution to this problem, and in order to record interpretable, repeatable, reproducible and comparable spectra, the measurements were conveyed under similar experimental conditions and spots inside the cell. In addition, the spectral region of the vibrations from the symmetric stretching of CH$_3$ (2935 cm^{-1}) and CH$_2$ (2854 cm^{-1}) and their intensities were evaluated to assume the proper focusing spot for the measurements

(Figure 3 and Table 2). Namely, space resolved Raman spectra of contrasting lipid rich regions (lipid bodies, cleavage furrow)[13,34] and the cytoplasm pointed to the augmented intensity of the bands around 2850 cm^{-1} with increased lipid concentration in the lipid bilayer of the plasma membrane as opposed to decrease of its band intensity in the cytoplasm spectrum. Also, the symmetric stretching bands of CH$_3$ (2935 cm^{-1}) and CH$_2$ (2854 cm^{-1}) are much more intense in lipid rich regions than in the cytoplasm due to a lower density of CH$_2$ groups in proteins compared to lipids. Considering this effect, it can be assumed that the recorded spontaneous Raman spectra and the respective bands in our experiments arise from the region of the cytoplasm.[13,34] As expected, the bands in the spectral region of the symmetric CH$_3$ stretchings (2935 cm^{-1}) and CH$_2$ stretchings (2854 cm^{-1}) are much more intense in the spectrum of the liposomes compared to the collected spectra of either the cells incubated with liposomes or control cells (Figure 3).

The label-free spectra of the hCmec/D3 cells (C), the liposomes (L), and the cells incubated with liposomes (CL) showed distinct variations in the region 1150–1030 cm^{-1} (C–C stretch of lipids) (Figure 3). The cell spectrum exhibits three distinct peaks at 1066 cm^{-1}, 1099 cm^{-1} and 1124 cm^{-1} (Table 2). The peaks at 1066 cm^{-1} and 1124 cm^{-1} are assigned as out of phase and in phase trans conformers (so called trans markers) while the peak at 1099 cm^{-1} is tentatively assigned to appear from the gauche conformer.[19] The C–C stretching region in the liposome (L) presented by a broad peak centered at 1087 cm^{-1} indicates a larger gauche content and probable superposition with the trans indicators. Further, the spectra of cells incubated with liposomes (CL) distinguishes itself from the spectra of the control cells (C) by the presence of a much more prominent gauche conformer band which expands toward lower and higher wavenumbers resembling the band in the liposomes.
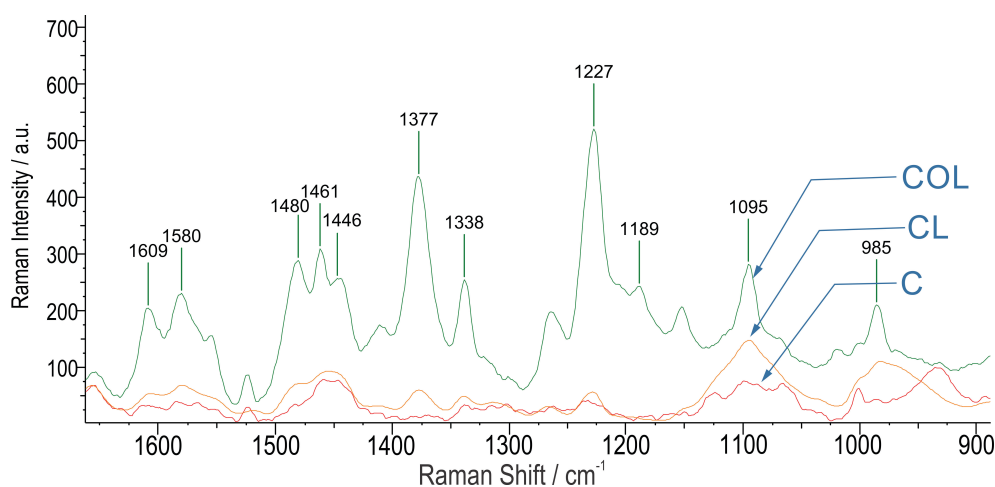

Figure 5. Raman spectra of control cells (C); cells incubated with label-free liposomes (CL); and cells incubated with Oil Red O labeled liposomes (COL).

Another important feature is a rather strong signal at 981 cm^{-1} in the spectra of the cells incubated with liposomes (CL), associated with O−C−C−N$^+$ stretching vibrations of the polar head groups[17] (Figure 3 and Table 2). This key band characteristic for phosphatidylcholine/cholesterol liposomes may be important for studying their internalization due to the absence of the strong signals associated with the vibrations of the choline head groups in the spectra of the control cells. The C−N stretching vibration is not pure and depends upon the conformation of the O−C−C−N$^+$ backbone, hence, samples with different conformation can be differentiated. Cholesterol symmetric C=C stretching band[18] appeared in the spectra of all three samples: the liposomes (1657 cm^{-1}), control cells (1655 cm^{-1}) and cells incubated with liposomes (1655 cm^{-1}) (Figure 3 and Table 2).

CONCLUSION

Raman spectroscopy is a versatile characterization technique that could be employed in almost every stage of the development and production of drug delivery systems. Herein, we demonstrated its capability for detection of label and label-free nanoliposomal carriers in an hCmec/D3 *in vitro* cell culture experiments that constitute an established *in vitro* BBB model, which is an important tool in the early phase of the development of drug delivery systems.

Eliminating the post-processing procedure, as labeling of drug-delivery carriers in such experiments, presents significant advantage both in sparing resources and preserving the original chemical and physical properties of the carrier surface. The data from our experiments clearly pointed out the unique Raman spectral features for detecting both labeled and label-free nanoliposomal carriers located inside the cells, which is very important taking into consideration the complexity of the matrix (cell environment) and the chemical similarity among the liposomal carriers and certain cell components. The valuable data gathered from this study could be further used in conjunction with multivariate analysis for label-free intracellular localization or quantitative cellular uptake of nano-sized drug delivery systems.

Supplementary Information. Supporting information to the paper is attached to the electronic version of the article at: https://doi.org/10.5562/cca3912.

PDF files with attached documents are best viewed with Adobe Acrobat Reader which is free and can be downloaded from Adobe's web site.

REFERENCES

[1] M. E. Keating, H. J. Byrne, *Nanomedicine* **2013**, *8*, 1335–1351.
https://doi.org/10.2217/nnm.13.108

[2] G. Bozzuto, A. Molinari, *Int. J. Nanomed.* **2015**, *10*, 975–999.
https://doi.org/10.2147/IJN.S68861

[3] B. Yu, H. C. Tai, W. Xue, L. J. Lee, R. J. Lee, *Mol. Membr. Biol.* **2010**, *27*, 286–298.
https://doi.org/10.3109/09687688.2010.521200

[4] K. M. Aguilar-Pérez, J. I. Avilés-Castrillo, D. I. Medina, R. Parra-Saldivar, H. M. N. Iqbal, *Front. Bioeng. Biotechnol.* **2020**, *8*, Article 579536.
https://doi.org/10.3389/fbioe.2020.579536

[5] S. Vranic, N. Boggetto, V. Contremoulins, S. Mornet, F. Marano, A. Squiban, S. Boland, *Part. Fibre Toxicol.* **2013**, *10*, 1–16.
https://doi.org/10.1186/1743-8977-10-2

[6] A. Ostrowski, D. Nordmeyer, A. Boreham, C. Holzhausen, L. Mundhenk, C. Graf, M. C. Meinke, A. Vogt, S. Hadam, J. Lademann, E. Ruhl, U. Alexiev, A. D. Gruber, *Beilstein J. Nanotechnol.* **2015**, *6*, 263–280.
https://doi.org/10.3762/BJNANO.6.25

[7] A. L. Robson, P. C. Dastoor, J. Flynn, W. Palmer, A. Martin, D. W. Smith, A. Woldu, S. Hua, *Front. Pharmacol.* **2018**, *9*, Article 80.
https://doi.org/10.3389/FPHAR.2018.00080

[8] H. C. Ishikawa-Ankerhold, R. Ankerhold, G. P. C. Drummen, *Molecules* **2012**, *17*, 4047–4132.
https://doi.org/10.3390/MOLECULES17044047

[9] U. S. Huth, R. Schubert, R. Peschka-Süss, *J. Controlled Release* **2006**, *110*, 490–504.
https://doi.org/10.1016/J.JCONREL.2005.10.018

[10] H. J. Byrne, F. Bonnier, E. Efeoglu, C. Moore, J. McIntyre, *Front. Bioeng. Biotechnol.* **2020**, *8*, Article 544311.
https://doi.org/10.3389/FBIOE.2020.544311

[11] K. Majzner, A. Kaczor, N. Kachamakova-Trojanowska, A. Fedorowicz, S. Chlopicki, M. Baranska, *Analyst* **2013**, *138*, 603–607.
https://doi.org/10.1039/c2an36222h

[12] C. Matthäus, C. Matthaus, T. Chernenko, C. Stiebing, L. Quintero, M. Miljković, L. Milane, A. Kale, M. Amiji, S. Lorkowski, V. Torchilin, J. Popp, M. Diem, *Springer Ser. Surf. Sci.* **2018**, *66*, 273–305.
https://doi.org/10.1007/978-3-319-75380-5_13

[13] G. Romero, E. Rojas, I. Estrela-Lopis, E. Donath, S. E. Moya, *Nanoscale Res. Lett.* **2011**, *6*, 1–4.
https://doi.org/10.1186/1556-276X-6-429

[14] D. Shalabalija, L. Mihailova, M. Simonoska Crcarevska, I. Cvetkovikj Karanfilova, V. Ivanovski, A. Kapedanovska Nestorovska, G. Novotni, M. Glavas Dodov, *J. Drug Delivery Sci. Technol.* **2021**, *63*, Article 102434.
https://doi.org/10.1016/J.JDDST.2021.102434

[15] M. R. Mozafari, M. H. Zareie, E. Piskin, V. Hasirci, *Drug Delivery* **2009**, *5*, 135–141.
https://doi.org/10.3109/10717549809031389

[16] S. Mourtas, A. N. Lazar, E. Markoutsa, C. Duyckaerts, S. G. Antimisiaris, *Eur. J. Med. Chem.* **2014**, *80*, 175–183. https://doi.org/10.1016/J.EJMECH.2014.04.050

[17] V. Živanović, A. Milewska, K. Leosson, J. Kneipp, *Anal. Chem.* **2021**, *93*, 10106–10113.
https://doi.org/10.1021/acs.analchem.1c00964

[18] R. Tantipolphan, T. Rades, C. J. Strachan, K. C. Gordon, N. J. Medlicott, *J. Pharm. Biomed. Anal.* **2006**, *41*, 476–484.
https://doi.org/10.1016/J.JPBA.2005.12.018

[19] C. B. Fox, R. H. Uibel, J. M. Harris, *J. Phys. Chem. B* **2007**, *111*, 11428–11436.
https://doi.org/10.1021/JP0735886

[20] A. Fujii, E. Fujimaki, T. Ebata, N. Mikami, *J. Chem. Phys.* **2000**, *112*, 6275–6284.
https://doi.org/10.1063/1.481272

[21] B. P. Gaber, P. Yager, W. L. Peticolas, *Biophys. J.* **1978**, *21*, 161–176.
https://doi.org/10.1016/S0006-3495(78)85516-7

[22] R. K. Bista, R. F. Bruch, University of Nevada, Reno, **2009**. Accessed: Jan. 22, 2022. [Online]. Available: https://scholarworks.unr.edu//handle/11714/4046

[23] V. V. Kuzmin, V. S. Novikov, L. Y. Ustynyuk, K. A. Prokhorov, E. A. Sagitova, G. Y. Nikolaeva, *J. Mol. Struct.* **2020**, *1217*, 128331.
https://doi.org/10.1016/J.MOLSTRUC.2020.128331

[24] Z. Varga, J. Mihály, S. Berényi, A. Bóta, *Eur. Polym. J.* **2013**, *49*, 2415–2421.
https://doi.org/10.1016/J.EURPOLYMJ.2013.02.025

[25] D. Yamini, G. D. Venkatasubbu, J. Kumar, V. Ramakrishnan, *Spectrochim. Acta, Part A* **2014**, *117*, 299–303. https://doi.org/10.1016/J.SAA.2013.07.064

[26] T. Rizk, C. Montero-Menei, C. Jollivet, J. P. Benoit, P. Menei, *J. Biomed. Mater. Res., Part A* **2004**, *68*, 360–364. https://doi.org/10.1002/JBM.A.20060

[27] N. A. Kraus, F. Ehebauer, B. Zapp, B. Rudolphi, B. J. Kraus, D. Kraus, *Adipocyte* **2016**, *5*, 351–358.
https://doi.org/10.1080/21623945.2016.1240137

[28] J. Thomas Bell, *Stain Technol.* **2009**, *34*, 219–221.
https://doi.org/10.3109/10520295909114678

[29] L. Li, H. W. Gao, J. R. Ren, L. Chen, Y. C. Li, J. F. Zhao, H. P. Zhao, Y. Yuan, *BMC Struct. Biol.* **2007**, *7*, 1–9.
https://doi.org/10.1186/1472-6807-7-16

[30] Y. Ou, T. Ou, L. Pei, K. Lai, Y. Huang, B. A. Rasco, X. Wang, Y. Fan, *Food Anal. Methods 2016 103* **2016**, *10*, 565–574.
https://doi.org/10.1007/S12161-016-0618-Z

[31] B. Çatıkkaş, *Period. Eng. Nat. Sci.* **2017**, *5*, 237–244.
https://doi.org/10.21533/pen.v5i2.139

[32] S. Dhakal, W. F. Schmidt, M. Kim, X. Tang, Y. Peng, K. Chao, *Foods* **2019**, *8*, Article 143.
https://doi.org/10.3390/FOODS8050143

[33] J. Coates, *Encyclopedia of Analytical Chemistry Vol. 12*. John Wiley & Sons, Ltd, Sep. 15, **2001**.
https://doi.org/10.3109/09687688.2010.521200

[34] J. F. Hsu, P. Y. Hsieh, H. Y. Hsu, S. Shigeto, *Sci. Rep.* **2015**, *5*, 1–8.
https://doi.org/10.1038/srep17541

[35] C. J. Frankt, R. I. Mccreey, D. C. B. Redd, *Anal. Chem.* **1995**, *67*, 7–26.
https://doi.org/10.1021/ac00101a001

[36] N. Stone, C. Kendall, J. Smith, P. Crow, H. Barr, *Faraday Discuss.* **2004**, *126*, 141–157.
https://doi.org/10.1039/B304992B

[37] A. W. Auner J. C. Thomas, *Biochem. Anal. Biochem.* **2016**, *5*, Article 1000284.
https://doi.org/10.4172/2161-1009.1000284

[38] L. Pei, Y. Ou, W. Yu, Y. Fan, Y. Huang, K. Lai, *J. Nanomater.* **2015**, *2015*, Article 430925.
https://doi.org/10.1155/2015/430925.34

[39] I. Notingher, S. Verrier, S. Haque, J. M. Polak, L. L. Hench, *Biopolymers* **2003**, *72*, 230–240.
https://doi.org/10.1002/BIP.10378

[40] W. T. Cheng, M. T. Liu, H. N. Liu, S. Y. Lin, *Microsc. Res. Tech.* **2005**, *68*, 75–79.
https://doi.org/10.1002/JEMT.20229

[41] C. Chen, F. Peng, Q. Cheng, D. Xu, 4th International Conference on Bioinformatics and Biomedical Engineering, 2010, pp. 1–4.
https://doi.org/10.1109/ICBBE.2010.5517260

[42] S. Dhakal, W. F. Schmidt, M. Kim, X. Tang, Y. Peng, K. Chao, *Foods* **2019**, *8*, Article 143.
https://doi.org/10.3390/FOODS8050143

[43] Z. Movasaghi, S. Rehman, I. U. Rehman, *Appl. Spectrosc. Rev.* **2007**, *42*, 493–541.
https://doi.org/10.1080/05704920701551530

[44] A. J. Hobro, M. Rouhi, E. W. Blanch, G. L. Conn, *Nucl. Acids Res.* **2007**, *35*, 1169–1177.
https://doi.org/10.1093/nar/gkm012